
Research Articles: Systems/Circuits

Network architecture underlying basal autonomic outflow: Evidence from frontotemporal dementia

Virginia E. Sturm¹, Jesse A. Brown¹, Alice Y. Hua², Sandy J. Lwi², Juan Zhou³, Florian Kurth⁴, Simon B. Eickhoff^{5,6}, Howard J. Rosen¹, Joel H. Kramer¹, Bruce L. Miller¹, Robert W. Levenson² and William W. Seeley^{1,7}

¹Department of Neurology; University of California, San Francisco; Sandler Neurosciences Center; 675 Nelson Rising Lane, Suite 190; San Francisco, CA 94158, USA.

²Department of Psychology, University of California, 3210 Tolman Hall #1650, Berkeley, CA 94720-1650, USA.

³Center for Cognitive Neuroscience, Neuroscience and Behavioral Disorders Program, Duke-National University of Singapore Medical School, 8 college road, Singapore, Singapore 169857.

⁴Cousins Center for Psychoneuroimmunology, Semel Institute for Neuroscience and Human Behavior, Department of Psychiatry and Biobehavioral Sciences, UCLA School of Medicine, Medical Plaza 300, Los Angeles, CA 90095, USA.

⁵Institute of Systems Neuroscience, Medical Faculty, Heinrich Heine University Düsseldorf, Düsseldorf, Germany

⁶Institute of Neuroscience and Medicine, Brain & Behaviour (INM-7), Research Centre Jülich, Jülich, Germany

⁷Department of Pathology, University of California, San Francisco, CA 94143, USA.

DOI: 10.1523/JNEUROSCI.0347-18.2018

Received: 5 February 2018

Revised: 23 August 2018

Accepted: 27 August 2018

Published: 4 September 2018

Author contributions: V.E.S., R.W.L., and W.W.S. designed research; V.E.S., J.A.B., A.Y.H., S.J.L., J.Z., F.K., S.B.E., H.J.R., J.H.K., and B.L.M. performed research; V.E.S., J.A.B., J.Z., F.K., and S.B.E. analyzed data; V.E.S. wrote the first draft of the paper; V.E.S., J.A.B., A.Y.H., S.J.L., J.Z., F.K., H.J.R., J.H.K., B.L.M., R.W.L., and W.W.S. edited the paper; V.E.S., R.W.L., and W.W.S. wrote the paper.

Conflict of Interest: The authors declare no competing financial interests.

This project was supported by grants from the NIH National Institute on Aging (P50AG023501, P01AG019724, R01AG052496, R01AG032306, R01AG057204, 1K23AG040127, and 1K23AG045289), The Larry L. Hillblom Foundation (2013-A-029-SUP and 2005/2T), the John Douglas French Foundation; the Consortium for Frontotemporal Dementia Research, and the Tau Consortium. We are grateful for the patients, healthy controls, and families that have participated in our research studies.

Corresponding Author: William W. Seeley, M.D., UCSF Memory and Aging Center - Box 1207, Sandler Neurosciences Center, 675 Nelson Rising Lane, Suite 190, San Francisco, CA 94158, Phone: (415) 476-2793 Fax: (415) 476-0213

Cite as: J. Neurosci ; 10.1523/JNEUROSCI.0347-18.2018

Alerts: Sign up at www.jneurosci.org/cgi/alerts to receive customized email alerts when the fully formatted version of this article is published.

1 Running Title: AUTONOMIC NETWORK ARCHITECTURE

2

3 Network architecture underlying basal autonomic outflow:

4 Evidence from frontotemporal dementia

5

6 Virginia E. Sturm¹

7 Jesse A. Brown¹

8 Alice Y. Hua²

9 Sandy J. Lwi²

10 Juan Zhou³

11 Florian Kurth⁴

12 Simon B. Eickhoff^{5,6}

13 Howard J. Rosen¹

14 Joel H. Kramer¹

15 Bruce L. Miller¹

16 Robert W. Levenson^{2*}

17 William W. Seeley^{1,7*}

18

19 ¹Department of Neurology; University of California, San Francisco; Sandler Neurosciences
20 Center; 675 Nelson Rising Lane, Suite 190; San Francisco, CA 94158, USA.

21
22 ²Department of Psychology, University of California, 3210 Tolman Hall #1650, Berkeley, CA
23 94720-1650, USA.

24
25 ³Center for Cognitive Neuroscience, Neuroscience and Behavioral Disorders Program, Duke-
26 National University of Singapore Medical School, 8 college road, Singapore, Singapore 169857.

27
28 ⁴Cousins Center for Psychoneuroimmunology, Semel Institute for Neuroscience and Human
29 Behavior, Department of Psychiatry and Biobehavioral Sciences, UCLA School of Medicine,
30 Medical Plaza 300, Los Angeles, CA 90095, USA.

31
32 ⁵Institute of Systems Neuroscience, Medical Faculty, Heinrich Heine University Düsseldorf,
33 Düsseldorf, Germany

34 ⁶Institute of Neuroscience and Medicine, Brain & Behaviour (INM-7), Research Centre Jülich,
35 Jülich, Germany

36

37 ⁷Department of Pathology, University of California, San Francisco, CA 94143, USA.

38

39 * authors contributed equally to the work

40

41 Corresponding Author:

42 William W. Seeley, M.D.

43 UCSF Memory and Aging Center - Box 1207

44 Sandler Neurosciences Center

45 675 Nelson Rising Lane, Suite 190

46 San Francisco, CA 94158

47 Phone: (415) 476-2793 Fax: (415) 476-0213

48

49 Number of pages: 53

50 Number of figures: 5

51 Number of tables: 5

52 Number of words (Abstract): 250

53 Number of words (Introduction): 647

54 Number of words (Discussion): 1511

55

56 Conflict of interest: None

57

58 Acknowledgements: This project was supported by grants from the NIH National Institute on

59 Aging (P50AG023501, P01AG019724, R01AG052496, R01AG032306, R01AG057204,

60 1K23AG040127, and 1K23AG045289), The Larry L. Hillblom Foundation (2013-A-029-SUP

61 and 2005/2T), the John Douglas French Foundation; the Consortium for Frontotemporal

62 Dementia Research, and the Tau Consortium. We are grateful for the patients, healthy controls,

63 and families that have participated in our research studies.

64

65

Abstract

66 The salience network is a distributed neural system that maintains homeostasis by regulating
67 autonomic nervous system activity and social-emotional function. Here we examined how
68 within-network connectivity relates to individual differences in human (including males and
69 females) baseline parasympathetic and sympathetic nervous activity. We measured resting
70 autonomic nervous system physiology in 24 healthy controls and 23 patients with behavioral
71 variant frontotemporal dementia (bvFTD), a neurodegenerative disease characterized by baseline
72 autonomic deficits. Participants also underwent structural and task-free functional magnetic
73 resonance imaging. First, we used voxel-based morphometry to determine whether salience
74 network atrophy was associated with lower baseline respiratory sinus arrhythmia (RSA; a
75 parasympathetic measure) and skin conductance level (SCL; a sympathetic measure) in bvFTD.
76 Next, we examined whether functional connectivity deficits in 21 autonomic-relevant, salience
77 network node-pairs related to baseline autonomic dysfunction. Lower baseline RSA was
78 associated with smaller volume in left ventral anterior insula (vAI), weaker connectivity between
79 bilateral vAI and bilateral anterior cingulate cortex (ACC), and stronger connectivity between
80 bilateral ACC and bilateral hypothalamus/amygdala. Lower baseline SCL, in contrast, was
81 associated with smaller volume in inferior temporal gyrus, dorsal mid-insula, and hypothalamus;
82 weaker connectivity between bilateral ACC and right hypothalamus/amygdala; and stronger
83 connectivity between bilateral dorsal anterior insula and periaqueductal gray. Our results suggest
84 that baseline parasympathetic and sympathetic tone depend on the integrity of lateralized
85 salience network hubs (left vAI for parasympathetic and right hypothalamus/amygdala for
86 sympathetic) and highly calibrated ipsilateral and contralateral network connections. In bvFTD,
87 deficits in this system may underlie resting parasympathetic and sympathetic disruption.

88

89 Significance Statement

90 The salience network maintains homeostasis and regulates autonomic nervous system activity.
91 Whether within-network connectivity patterns underlie individual differences in resting
92 parasympathetic and sympathetic nervous system activity, however, is not well understood. We
93 measured baseline autonomic nervous system activity in healthy controls and patients with
94 behavioral variant frontotemporal dementia, a neurodegenerative disease characterized by resting
95 autonomic deficits, and probed how salience network dysfunction relates to diminished
96 parasympathetic and sympathetic outflow. Our results indicate that baseline parasympathetic and
97 sympathetic tone are the product of complex, opposing intra-network nodal interactions and
98 depend on the integrity of highly tuned, lateralized salience network hubs (i.e., left ventral
99 anterior insula for parasympathetic activity and right hypothalamus/amygdala for sympathetic
100 activity).

101

102

Introduction

103 The salience network is a distributed brain system that produces emotions and monitors
104 the dynamic conditions of the body (Seeley et al., 2007). With hubs in ventral anterior insula
105 (vAI) and anterior cingulate cortex (ACC) and tight connections with ventral striatum and central
106 pattern generators including the hypothalamus, amygdala, and periaqueductal gray (PAG), the
107 salience network participates in and may coordinate autonomic nervous system (ANS)
108 regulation. During emotions, the salience network triggers visceromotor changes that disrupt
109 quiescence and move an organism from rest to action. At rest, the salience network adjusts the
110 internal milieu to meet current metabolic and motivational conditions (Benarroch, 1993;
111 Carmichael and Price, 1995; Ongur and Price, 2000; Saper, 2002; Barbas et al., 2003a; Critchley,
112 2005; Beissner et al., 2013; Critchley and Harrison, 2013). A continuous stream of sensory
113 information travels from the spinal cord through the brainstem via the lamina I spinothalamic
114 pathway and vagal afferents. This interoceptive information is then relayed to the dorsal
115 posterior insula, mid-insula, and onward to vAI, a physiological integration site that is thought to
116 represent internal feeling states that color subjective emotional experience and shape behavior
117 (Craig, 2002; Critchley, 2004; Craig, 2009; Damasio and Carvalho, 2013).

118 The salience network influences both the sympathetic and parasympathetic branches of
119 the ANS. The sympathetic ANS (SANS) responds to arousing or threatening stimuli and
120 mobilizes behavior (Saper, 2002). The parasympathetic ANS (PANS), in contrast, downregulates
121 arousal via the inhibitory influence of the vagus nerve. The vagus sends efferent signals from the
122 brain to the internal organs, reducing heart rate to a pace that is slower than that set by the
123 sinoatrial node (Carlson et al., 1992; Levy et al., 1993; Saper, 2002; Thayer and Siegle, 2002)
124 and creating a “rest and digest” state that fosters interpersonal engagement and emotional

125 attunement (Porges, 2001). These two ANS branches appear to be asymmetrically organized in
126 the brain. While right-lateralized (i.e., non-dominant hemisphere) neural pathways promote
127 SANS outflow, left-lateralized (i.e., dominant hemisphere) systems facilitate PANS activity
128 (Oppenheimer et al., 1992; Oppenheimer et al., 1996; Yoon et al., 1997; Wittling et al., 1998a;
129 Wittling et al., 1998b; Craig, 2005; Guo et al., 2016).

130 Although previous research has examined how salience network connectivity relates to
131 PANS activity (Guo et al., 2016), it remains unknown how within-network nodal interactions
132 relate to individual differences in resting PANS and SANS function. The behavioral variant of
133 frontotemporal dementia (bvFTD) is a neurodegenerative disease that targets the salience
134 network (Seeley et al., 2007; Zhou et al., 2010) and offers a unique opportunity to examine how
135 salience network integrity relates to ANS deficits. In bvFTD there is progressive deterioration of
136 social behavior, empathy, and emotion (Rascovsky et al., 2007; Seeley et al., 2008; Kumfor and
137 Piguet, 2012; Seeley et al., 2012; Barsuglia et al., 2014; Joshi et al., 2014b; Levenson et al.,
138 2014; Mendez et al., 2014). In addition to deficits in emotion generation (Sturm et al., 2006;
139 Sturm et al., 2008; Eckart et al., 2012), patients with bvFTD also exhibit PANS and SANS
140 deficits at rest (Joshi et al., 2014a; Guo et al., 2016).

141 In the present study, we investigated whether specific patterns of salience network
142 dysfunction related to resting PANS and SANS deficits. We measured baseline ANS activity in
143 patients with bvFTD and healthy controls (HC) during a laboratory-based testing session.
144 Participants also underwent structural magnetic resonance imaging (MRI) and task-free
145 functional MRI (fMRI). Building on previous studies (Benarroch, 1993; Thayer and Lane, 2000;
146 Craig, 2002; Saper, 2002; Seeley et al., 2012; Critchley and Harrison, 2013; Damasio and
147 Carvalho, 2013), we developed a neural systems model (Figure 1A) to guide our examination of

AUTONOMIC NETWORK ARCHITECTURE

148 nodes and edges (i.e., connectivity between node-pairs) that are embedded in the salience
149 network and support ANS activity. We hypothesized that lateralized network impairment would
150 be associated with resting ANS deficits such that left-sided dysfunction would predict
151 diminished PANS activity whereas right-sided dysfunction would predict lower SANS activity.

152 Materials and Methods

153 *Participants*

154 We included 47 participants in the present study: 24 HC (56.7 – 79.6 years of age) and 23
155 patients with bvFTD (34.2 – 71.2 years of age) (Rascovsky et al., 2007). The HC were recruited
156 from advertisements and were free of current or previous neurological or psychiatric disorders.
157 Patients underwent an interdisciplinary team evaluation at the University of California, San
158 Francisco (UCSF) Memory and Aging Center that included a clinical interview, neurological
159 exam, functional assessment, MRI, and neuropsychological testing (Table 1). A functional
160 assessment of dementia severity was obtained using the Clinical Dementia Rating Scale (CDR)
161 (Morris, 1993). Body mass index (BMI) was calculated for all patients and for 20/21 of HC with
162 available height and weight data. Participants were not taking medications at the time of the
163 laboratory assessment (described below) that could significantly affect ANS functioning (i.e.,
164 stimulants, beta-blockers, or acetylcholinesterase inhibitors). Power calculations based on
165 previous studies of ANS dysfunction in bvFTD (Joshi et al., 2014a; Guo et al., 2016) showed
166 that an $\alpha = .05$ level test in a sample of this size had power greater than 80% to detect a difference
167 between the groups.

168 *Experimental Design and Statistical Analysis*169 *Laboratory Assessment of Autonomic Physiology*

170 *Procedure.* After informed consent, participants' physiological functioning was assessed
171 at the Berkeley Psychophysiology Laboratory at the University of California, Berkeley
172 (Levenson et al., 2008).

173 *Resting Baseline Autonomic Physiology.* Eleven 35-second resting baseline periods were
174 extracted from a task in which participants viewed 11 short films; for complete details, see
175 previous task descriptions (Goodkind et al., 2015). During these pre-film baseline periods,
176 participants were instructed to relax and to watch an "X" on a white monitor screen.

177 *Measures.* Physiological measures were monitored continuously using a Grass Model 7
178 or Biopac polygraph, a computer with analog-to-digital capability, and an online data acquisition
179 and analysis software package written by Robert W. Levenson. The software computed second-
180 by-second averages for the following measures: (1) heart rate (Beckman miniature electrodes
181 with Redux paste were placed in a bipolar configuration on opposite sides of the participant's
182 chest; the inter-beat interval was calculated as the interval, in milliseconds, between successive R
183 waves); (2) respiratory sinus arrhythmia (RSA), the peak-valley method was used, which
184 measures the time differences between the shortest inter-beat interval during inspiration and the
185 longest inter-beat interval during expiration on each breath (Grossman et al., 1990); (3) skin
186 conductance level (SCL), a constant-voltage device was used to pass a small voltage between
187 Beckman regular electrodes (using an electrolyte of sodium chloride in Unibase) attached to the
188 palmar surface of the middle phalanges of the ring and index fingers of the non-dominant hand;
189 (4) respiration period (a pneumatic bellows was stretched around the thoracic region and the
190 inter-cycle interval was measured in milliseconds between successive inspirations); and (5)
191 finger temperature (a thermistor attached to the distal phalanx of the little finger of the non-
192 dominant hand recorded temperature in degrees Fahrenheit).

193 This array of measures was selected to sample from major ANS (cardiovascular,
194 electrodermal, and respiratory) systems and enabled us to examine both PANS and SANS
195 integrity. RSA is a measure of vagally-mediated, beat-to-beat variation in heart rate, an index of
196 PANS activity (Berntson et al., 1997). RSA is closely linked to respiration, with heart rate
197 decelerating during expiration and accelerating during inspiration. We used the peak-valley
198 method, which quantifies the difference between the longest heart period during expiration and
199 the shortest heart period during inspiration (Grossman et al., 1990; Grossman and Taylor, 2007).
200 The natural logarithm of RSA (lnRSA) was used to improve proximity to a normal distribution
201 and was used in all analyses. SCL, which increases as there is greater innervation of the eccrine
202 sweat glands, is a relatively pure SANS measure (Critchley, 2002). Heart rate, respiration period,
203 and temperature are influenced by both ANS branches and, therefore, were not the focus of our
204 neuroimaging analyses.

205 Mean levels of physiological responding were computed for each 33-second pre-film
206 baseline (one second at the beginning and end of each baseline and trial were omitted to account
207 for measurement error in the timing of trial onset and offset) and were then averaged across all
208 11 baseline trials. We calculated a Cronbach's alpha reliability coefficient for each channel and
209 found high reliability for each measure across the 11 baseline periods (inter-beat interval=.99,
210 RSA=.94, SCL=.99, respiration period=.92, and temperature=.99), which suggests that the
211 overall baseline means were an accurate reflection of stable, trait-like baseline ANS physiology.

212 *Image Acquisition*

213 *Structural Imaging.* The majority of participants (17 HC and 22 patients) underwent
214 research-quality MRI within close proximity of the laboratory assessment of autonomic

215 physiology (4 months for patients and 12 months for HC). Structural images were obtained on a
216 3.0 Tesla Siemens (Siemens, Iselin, NJ) TIM Trio scanner equipped with a 12-channel head coil
217 located at the UCSF Neuroscience Imaging Center. Whole brain images were acquired using
218 volumetric MPRAGE (acquisition time=8:53, sagittal orientation, a field of view of 160 x 240 x
219 256 mm with an isotropic voxel resolution of 1 mm³, TR=2300 ms, TE=2.98 ms, TI=900 ms, flip
220 angle=9°).

221 *Functional Imaging.* Task-free fMRI scans were also obtained in 14 HC and 17 patients
222 with bvFTD. The 3T scanner acquired 240 task-free T2*-weighted echoplanar fMRI volumes
223 (acquisition time=8:06, axial orientation with interleaved ordering, field of view=230 x 230 x
224 129 mm, matrix size=92 x 92, effective voxel resolution=2.5 x 2.5 x 3.0 mm, TR=2000 ms,
225 TE=27 ms)

226 *Image Preprocessing*

227 *Structural Imaging.* Structural T1 images were visually inspected for movement artifacts
228 before being processed with SPM12 (<http://www.fil.ion.ucl.ac.uk/spm/software/spm12/>). One
229 patient was excluded due to poor scan quality, leaving a total of 21 bvFTD and 17 HC. Within
230 the same generative model (Ashburner and Friston, 2005), the T1-weighted images were
231 segmented into gray and white matter using the segment program in SPM12. To guarantee
232 voxel-wise comparability, gray matter images were normalized to Montreal Neurological
233 Institute (MNI) space by applying 12-parameter linear transformation and non-linear warping,
234 modulated, and smoothed with an 8 mm full-width at half-maximum Gaussian kernel.

235 *Functional Imaging.* For each fMRI scan, the first five volumes were discarded. SPM12
236 and FSL (<http://fsl.fmrib.ox.ac.uk/fsl>) software were used for subsequent fMRI preprocessing.

237 The remaining 235 volumes were slice-time corrected, realigned to the mean functional image,
238 and assessed for rotational and translational head motion. Volumes were next co-registered to the
239 MP-RAGE image and then normalized to the standard MNI-152 healthy adult brain template
240 using SPM segment, producing MNI-registered volumes with 2 mm³ isotropic resolution. These
241 volumes were spatially smoothed with a 6 mm radius Gaussian kernel and temporally bandpass
242 filtered in the .008-.15 Hz frequency range using fslmaths. Nuisance parameters in the
243 preprocessed data were estimated for the cerebrospinal fluid (CSF) using a mask in the central
244 portion of the lateral ventricles and for the white matter (WM) using a mask of the highest
245 probability cortical WM as labeled in the FSL tissue prior mask. Additional nuisance parameters
246 included the 3 translational and 3 rotational motion parameters, the temporal derivatives of the
247 previous 8 terms (WM/CSF/6 motion), and the squares of the previous 16 terms (Satterthwaite et
248 al., 2013). Any participant with a maximum relative head translation greater than 3 mm,
249 maximum relative rotation greater than 3 degrees, or more than 10% of frames with a motion
250 spike greater than 1 mm, were excluded from the analysis. Previous work has shown that the
251 edges tested in the present study have moderate to good test-retest reliability with this level of
252 head movement excluded (Guo et al., 2012) and that resting state measures are reliable when
253 these preprocessing strategies are employed (Varikuti et al., 2017). We excluded two patients for
254 excessive motion, leaving 14 HC and 15 patients with bvFTD. The groups (controlling for age,
255 sex, and education) did not significantly differ on total head movement during the scan, $F(1,$
256 $24)= 1.43, p=.24, \eta_p^2=.06$.

257 *Analyses*

258 *Structural Neuroimaging Analyses.* We conducted separate whole-brain voxel-based
259 morphometry (VBM) analyses (Bates et al., 2003) in the patients to identify brain regions in

260 which smaller gray matter volume was associated with baseline RSA and SCL deficits in bvFTD
261 (Table 2). We chose to run the structural neuroimaging analyses in the patients only because they
262 have significantly more atrophy than the controls in many of the regions that we expected would
263 be related to the ANS measures and, thus, might unduly bias the analyses if we combined all of
264 the participants. Age, sex, education were included as nuisance covariates. In a follow-up
265 analysis, we added SCL as an additional covariate in the RSA analysis and RSA as an additional
266 covariate in the SCL analysis, which further allowed us to examine the independence of the
267 neural correlates of each measure. A priori significance was established at uncorrected $p < .001$.
268 One thousand permutation analyses using combined peak and extent thresholds were run to
269 derive a study-specific error distribution to determine the one-tailed T -threshold at $p_{FWE} < .05$,
270 corrected for multiple comparisons (Nichols and Holmes, 2002).

271 *Functional Connectivity Neuroimaging Analyses.* Using a graph theoretical framework,
272 we identified “connectivity clusters” that corresponded to the regions of interest (ROIs) in our
273 model (Figure 1B). The clusters were obtained from task-free fMRI data in an independent
274 cohort of 40 healthy older controls (20 males, all less than 66 years old) as previously described
275 (Guo et al., 2012). In brief, we used four vAI and dorsal anterior insula (dAI) seeds, drawn from
276 a meta-analysis of task-based fMRI studies that activated the insula (Kurth et al., 2010) to derive
277 four connectivity maps. These four maps were entered into a full-factorial analysis, which
278 identified brain regions with connectivity to the dAI clusters, to the vAI clusters, or to both the
279 dAI and vAI clusters. We extracted the blood-oxygen-level dependent (BOLD) time series from
280 21 clusters that corresponded to the ROIs in our *a priori* theoretical model (Figure 1A) and
281 created a matrix that consisted of the connectivity strength of the edges in that model. Because
282 the clusters are data-driven and have connectivity-based contours, they may sample a more

283 homogeneous functional signal and be better suited for matrix-based analyses than typical
284 spherical or landmark-based ROIs (Shirer et al., 2012).

285 We used previously established methods (Sturm et al., 2013) to identify key edges
286 associated with RSA and SCL. First, edges weights were *r*-to-*z* transformed, and we then ran
287 correlation analyses across the patients and controls between RSA and the connectivity strength
288 of all 210 edges in our matrix. We planned to include any regions for which the correlation
289 coefficient was greater than or equal to .20, a small to medium effect size (Cohen, 1992) and a
290 permissive inclusion threshold, as additional candidate predictor variables in subsequent
291 regression analyses. Next, we ran hierarchical regression analyses in order to determine which
292 edges were significant predictors of RSA, a conservative test of our hypotheses because edges
293 must emerge as significant predictors from a group of candidate predictor regions. In step one,
294 we entered age, sex, education, and diagnosis into the model. In step two, we used a “forward”
295 entry model to determine which edges accounted for a significant amount of variance above and
296 beyond the control variables; thus, edges that did not account for significant variance were
297 excluded from the model. In this second step, we included as predictor candidates all of the
298 edges that passed the .2 inclusion threshold from our correlation analyses. We ran three separate
299 regression analyses for ipsilateral left-hemisphere edges, ipsilateral right-hemisphere edges, and
300 edges that crossed to the contralateral hemisphere (i.e., left to right or right to left) to minimize
301 potential collinearity between homologous regions. We also examined our models to confirm
302 that there was only weak multicollinearity among variables (variance inflation factor < 4). We
303 next repeated this entire process to identify edges that were significant predictors of baseline
304 SCL. For each regression, we visually inspected the histogram and P-P plot of the standardized
305 residuals to ensure that the error terms were normally distributed. The plots showed that the

306 points generally followed the normal (diagonal) line with no outliers or strong deviations,
307 indicating that the assumptions of the regression models were met.

308 To ensure that any associations between functional connectivity and ANS physiology
309 were not due to atrophy, we conducted another set of hierarchical regression analyses for RSA
310 and SCL. From the structural scans, we extracted the total gray matter volume from each ROI.
311 Here, in addition to the other nuisance covariates (age, sex, education, and diagnosis), we also
312 included the mean ROI volumes for each of the edges (i.e., the mean volume of each node that
313 comprised the relevant edges) that had entered the original forward-entry regression models in
314 step one. In step two, we included the connectivity strength of the edges that had entered the
315 models in our original analyses.

316 We anticipated that any associations that we detected between ANS activity and
317 functional connectivity would reflect a general relationship that is not specific to either
318 diagnosis. To confirm that this was the case, we repeated the final regression models (for
319 ipsilateral left-hemisphere edges, ipsilateral right-hemisphere edges, and edges that crossed to
320 the contralateral hemisphere) for RSA and SCL in each diagnosis separately. Here, we included
321 age, sex, and education as nuisance covariates in step one. In step two, we entered the edges that
322 had explained a significant portion of the variance in the forward-entry regression models we had
323 conducted across the sample. Although each diagnostic group was much smaller than the total
324 sample and, thus, our power was substantially reduced in these analyses, our aim was to
325 investigate whether the effect sizes of any the associations between functional connectivity and
326 ANS activity that we detected across the sample were comparable in each of the diagnostic
327 groups when examined separately.

328 In a separate set of regressions, we examined whether the mean connectivity strength of
329 the edges that entered the regression RSA and SCL models were lower in bvFTD compared to
330 HC. In these analyses, the independent variable was diagnosis (bvFTD or HC), and the
331 covariates included age, sex, and years of education.

332 Results

333 *Smaller left vAI volume and lower vAI – ACC connectivity are associated with lower baseline*
334 *PANS activity*

335 In bvFTD, lower RSA was related to atrophy in a large cluster within left vAI, among
336 other regions (Table 3 and Figure 2A). When we also controlled for SCL in this RSA analysis,
337 the results remained largely unchanged though some regions that were more weakly associated
338 with RSA no longer remained significant (Table 3 and Figure 2B). Forward-entry hierarchical
339 regression analyses across the bvFTD and HC groups determined that weaker functional
340 connectivity in bilateral vAI – ACC edges, including left vAI – left ACC (2–5), left vAI – right
341 ACC (2–16), and right vAI – right ACC (13–15), was associated with lower baseline RSA
342 (Table 4 and Figure 2C). The functional connectivity results remained significant after atrophy
343 correction. When we repeated the original regression analyses in each diagnosis separately, there
344 were similar associations between RSA and the functional connectivity measures (Figure 4-1).
345 Patients with bvFTD had significantly lower connectivity strength than the HC in the right vAI –
346 right ACC (13–15) and left ACC – right amygdala (6–18) edges (Table 5). These findings
347 indicate that structural and functional deterioration of vAI (left > right) and its connections with
348 ACC are associated with a loss of basal parasympathetic tone as measured by RSA.

349 *Stronger connectivity in ACC – hypothalamus/amygdala edges relates to lower baseline PANS*
350 *activity*

351 Although lower RSA was associated with weaker vAI – ACC connectivity, the regression
352 analyses also revealed that lower RSA was associated with stronger connectivity in other edges.
353 Most notably, stronger connections between bilateral ACC and predominantly right-sided
354 hypothalamus/amygdala edges were associated with lower RSA (Table 4 and Figure 2C). This
355 pattern was not mirrored in the VBM analyses in that there were no regions where larger volume
356 was associated with lower RSA. All of the functional connectivity results held with atrophy
357 correction, with the exception of the right pregenual ACC – right hypothalamus ($p=.07$) and right
358 vAI – right hypothalamus ($p=.30$) edges. These results suggest that RSA depends on both
359 functional integrity of vAI – ACC edges and suppressed connectivity in ACC – hypothalamus
360 and ACC – amygdala edges (particularly in the right hemisphere), regions that appear to inhibit
361 PANS activity, perhaps by promoting SANS outflow.

362 *Stronger connectivity in ACC – hypothalamus/amygdala edges relates to higher SANS activity*

363 If the hypothalamus and amygdala promote SANS activity as suggested by the RSA
364 analyses, then we would expect that preserved volume and connectivity in these regions would
365 be associated with higher SCL. Consistent with this framework, larger volume in left inferior
366 temporal gyrus and left hypothalamus as well as right hypothalamus, amygdala and
367 periaqueductal gray (at a more permissive threshold of $p<.005$) was associated with higher SCL
368 (Table 3 and Figure 3A). Furthermore, when we also controlled for RSA in this SCL analysis,
369 the results remained largely unchanged though some regions that were more weakly associated
370 with SCL no longer remained significant (Table 3 and Figure 3B). Stronger bilateral ACC –

371 hypothalamus connectivity was also associated with higher baseline SCL (Table 4 and Figure
372 3C). Although there were no regions for which larger volume was associated with lower SCL,
373 stronger connectivity in bilateral dAI – PAG and left anterior midcingulate cortex (aMCC) –
374 right hypothalamus edges did relate to lower SCL (Table 4 and Figure 3C). All functional
375 connectivity results held with atrophy correction. When we repeated the original regression
376 analyses in each diagnosis separately, there were similar associations between SCL and the
377 functional connectivity measures (Figure 4-1). Taken together, these findings suggest that the
378 right hypothalamus in particular is a key hub in SANS outflow and that atrophy and diminished
379 connectivity in right hypothalamus/amygdala edges impede SCL. Patients with bvFTD had
380 significantly lower connectivity strength than the HC in the left ACC – right hypothalamus (6–
381 19), right ACC – right amygdala (16–18), right ACC – left ACC (17–5), right dAI – PAG (11–
382 21), and left aMCC – right hypothalamus (4–19) edges (Table 5). Visual inspection of the data
383 confirmed that significant associations that emerged between the functional connectivity
384 measures and ANS activity were not driven by group effects (Figure 4).

385 Discussion

386 The salience network coordinates the parasympathetic and sympathetic branches of the
387 ANS (Benarroch, 1993; Ongur and Price, 2000; Thayer and Lane, 2000; Saper, 2002; Seeley et
388 al., 2007; Beissner et al., 2013; Critchley and Harrison, 2013). This system enables the brain to
389 trigger changes in the periphery and to receive continuous feedback about the physiological
390 conditions of the body (Craig, 2002; Seeley et al., 2012; Critchley and Harrison, 2013). Previous
391 research has revealed cerebral hemispheric asymmetry in PANS and SANS neural systems
392 organization (Oppenheimer et al., 1992; Craig, 2005). Whereas the left hemisphere is essential
393 for PANS functioning (Wittling et al., 1998a; Guo et al., 2016), the right hemisphere plays a

394 dominant role in SANS activation (Yoon et al., 1997; Wittling et al., 1998b). In keeping with this
395 anatomical framework, our results suggest that healthy PANS and SANS activities are the
396 product of complex, opposing intra-network nodal interactions. We found that the structural and
397 functional integrity of specific hubs that have been identified in prior studies—left vAI for PANS
398 and right hypothalamus/amygdala for SANS (Xavier et al., 2013; Guo et al., 2016)—were
399 critical for maintaining resting ANS outflow. Although the left vAI and right
400 hypothalamus/amygdala hubs were lateralized and located in the predicted hemispheres, they had
401 connections with ipsilateral and contralateral network nodes that were also integral for baseline
402 ANS activity. While ipsilateral pathways may facilitate within-hemisphere generation of PANS
403 or SANS activity, contralateral projections may foster communication between hemispheres and
404 enable system-level integration of PANS and SANS information. A distributed, bilateral ANS
405 network that is anchored by asymmetric hubs may provide an efficient physiological system in
406 which opposing PANS and SANS influences remain in a dynamic equilibrium at rest but can
407 generate emotional reactions when needed.

408 *RSA depends on strong vAI – ACC integrity and weak ACC – hypothalamus/amygdala*
409 *connectivity*

410 Our analyses revealed a constellation of nodes and edges that were associated with
411 resting RSA. Consistent with previous findings, vAI and pregenual ACC emerged as key hubs of
412 PANS control (Oppenheimer et al., 1996; Gianaros et al., 2004; Thayer et al., 2012; Allen et al.,
413 2015; Guo et al., 2016; Jennings et al., 2016). Left vAI volume was positively associated with
414 RSA in the structural neuroimaging analyses, and stronger connectivity in left vAI edges was
415 also associated with higher RSA. vAI and pregenual ACC have tight reciprocal connections
416 (Mesulam and Mufson, 1982; Carmichael and Price, 1996) and send projections to ANS

417 brainstem nuclei including the nucleus ambiguus and dorsal motor nucleus of the vagus (Shipley,
418 1982; Hurley et al., 1991), a system that may promote the relay of PANS commands from
419 cortical and subcortical hubs to peripheral organs such as the heart (Gatti et al., 1996).

420 In addition to edges in which stronger connectivity was associated with higher RSA,
421 patients with weaker ACC – hypothalamus and ACC – amygdala connectivity had higher RSA.
422 Interestingly, stronger connectivity in ACC – hypothalamus and ACC – amygdala edges was
423 also associated with higher SCL, suggesting that the hypothalamus and amygdala (particularly in
424 the right hemisphere) are central pattern generators essential for SANS outflow (Barbas and De
425 Olmos, 1990; Laine et al., 2009; Xavier et al., 2013). Direct connections from ACC to the
426 intermediolateral cell column (Bacon and Smith, 1993), or indirect connections through
427 hypothalamus or amygdala (Saper et al., 1976; ter Horst et al., 1984; Barbas et al., 2003b), may
428 promote SANS outflow. Therefore, higher connectivity between these regions and ACC may
429 impede PANS activity by stimulating SANS outflow, consistent with prior studies showing an
430 antagonistic relation between PANS and SANS activity (Levy, 1990; Saku et al., 2014). Our
431 results suggest that RSA depends not only on strong connectivity in vAI – ACC, which promotes
432 vagal tone, but also on relatively weak, or suppressed, connectivity in ACC –
433 hypothalamus/amygdala, connections that encourage sympathetic outflow.

434 *SCL depends on ACC – hypothalamus/amygdala integrity and weak dAI – PAG connectivity*

435 Together with ACC, the amygdala and hypothalamus are integral SANS hubs (Bandler
436 and Carrive, 1988; An et al., 1998; Ongur et al., 1998; Price, 1999; Ongur and Price, 2000). Our
437 results indicate that stronger pregenual ACC – hypothalamus/amygdala connectivity was
438 associated with higher SCL. Larger volume in inferior temporal gyrus, hypothalamus, amygdala,

439 and periaqueductal gray, among other regions, also predicted greater SCL activity. The integrity
440 of pregenual ACC and its direct projections with hypothalamus and amygdala, therefore, appears
441 to be essential for SANS outflow (Barbas and De Olmos, 1990; Davis and Whalen, 2001;
442 Ghashghaei and Barbas, 2002; Laine et al., 2009).

443 Like RSA, SCL depended on stronger connectivity in some edges but weaker
444 connectivity in others. Lower bilateral dAI – PAG and left aMCC – right hypothalamus
445 connectivity was associated with higher SANS tone. Both aMCC and dAI are key structures in
446 an inhibitory control system that constrains cognition and behavior and may also downregulate
447 physiological arousal (Aron et al., 2004; Nee et al., 2007; Touroutoglou et al., 2012; Enriquez-
448 Geppert et al., 2013; Hoffstaedter et al., 2014). Through connections with lateral frontoparietal
449 task control networks (Mesulam and Mufson, 1982; Mufson and Mesulam, 1982), dAI plays a
450 central role in response inhibition and emotion suppression (Aron, 2007; Giuliani et al., 2011).
451 The structural and functional integrity of aMCC has been associated with greater heart rate
452 variability (Critchley et al., 2003; Winkelmann et al., 2016), and connectivity in this region,
453 therefore, may contribute to dampening, rather than inducing physiological arousal. Although we
454 were unable to examine substructures within our subcortical ROIs, this hypothesis would be
455 especially compelling if the connectivity strength from our PAG and hypothalamus ROIs
456 primarily captured the activity of their PANS-relevant subregions (Bandler and Shipley, 1994; da
457 Silva et al., 2003) (Figure 5). Weakened connectivity in a PANS-mediated visceromotor braking
458 system, therefore, may facilitate SANS activity. In bvFTD, atrophy and connectivity disruption
459 involving both PANS and SANS structures likely resulted in a net loss of RSA and SCL activity
460 despite altered intra-network nodal interactions.

461

Limitations

462 There are several limitations of the present study that should be considered. First, the HC
463 were older than the patients with bvFTD. Given that RSA and SCL decline in normal aging
464 (Barontini et al., 1997; Masi et al., 2007), the age distribution of our sample would work against
465 our hypothesis and make it more difficult for us to detect ANS impairment in the younger
466 clinical group. Furthermore, we took several additional steps to mitigate the potential impact of
467 age on our results: (1) our primary analyses were regression analyses rather than group
468 comparisons, which allowed us to investigate how brain volume and functional connectivity
469 related to ANS activity across the diagnostic groups, (2) we included age as a covariate in all
470 analyses, (3) we conducted a follow-up analysis on ANS activity in a subgroup of patients who
471 were age-matched and continued to find PANS and SANS deficits in bvFTD, a pattern that is
472 consistent with previous studies (Joshi et al., 2014a; Guo et al., 2016). We also found that
473 patients had faster baseline respiration rates, an alteration that may also reflect disruption of
474 vagal pathways (Carlson et al., 1992; Critchley, 2002; Rybak et al., 2004). Given that our sample
475 size was relatively small, additional studies are needed to detect the more subtle relationships
476 that might exist between functional connectivity and ANS outflow. Larger studies of bvFTD will
477 also be critical for elucidating whether RSA deficits relate to the alterations in respiration that we
478 detected. Second, our study was not able to examine the functional connectivity of many relevant
479 ANS brainstem nuclei, and many of our subcortical ROIs could have been deconstructed further
480 into anatomically meaningful subregions with specific PANS and SANS roles. The
481 hypothalamus and PAG, for example, can be divided into subregions that receive distinct
482 projections from ACC and vAI and play different roles in PANS and SANS (Bandler and
483 Shipley, 1994; Price, 1999). Because of this limitation, we may have failed to detect important
484 associations between these subregions and our ANS measures. Future studies that are able to

AUTONOMIC NETWORK ARCHITECTURE

485 subdivide these small structures into even finer parcels will continue to elucidate the neural
486 architecture of ANS functioning. Third, whereas our PANS measure, RSA, was a cardiovascular
487 measure, our SANS measure, SCL, was an electrodermal measure. Future studies that utilize
488 cardiovascular measures of SANS activity, such as impedance cardiography, could help to
489 determine whether all aspects of SANS activity are similarly disrupted in bvFTD or whether the
490 SANS impairment is specific to electrodermal outflow. Given that SCL is a cholinergic, rather
491 than an adrenergic, SANS measure, it is also possible that cholinergic dysfunction in bvFTD may
492 underlie both the RSA and SCL deficits that we detected. Whether the adrenergic system is also
493 altered in bvFTD will need to be addressed in future studies.

494

Conclusion

495 Although a single distributed neural network supports ANS physiology, opposing PANS
496 and SANS subsystems within this network play distinct roles in homeostasis maintenance. Our
497 results suggest that highly calibrated connections within the PANS and SANS subnetworks
498 promote ANS outflow. Disruption of these subsystems in bvFTD may tip the autonomic balance
499 and alter resting physiology as well as emotional responding. These findings may have wider
500 implications for the study of psychiatric conditions with alterations in emotion and behavior.

501

References

502 Allen B, Jennings JR, Gianaros PJ, Thayer JF, Manuck SB (2015) Resting high-frequency heart

503 rate variability is related to resting brain perfusion. *Psychophysiology* 52:277-287.

504 An X, Bandler R, Ongur D, Price JL (1998) Prefrontal cortical projections to longitudinal

505 columns in the midbrain periaqueductal gray in macaque monkeys. *J Comp Neurol*

506 401:455-479.

507 Aron AR (2007) The neural basis of inhibition in cognitive control. *The Neuroscientist* 13:214-

508 228.

509 Aron AR, Robbins TW, Poldrack RA (2004) Inhibition and the right inferior frontal cortex.

510 *Trends Cogn Sci* 8:170-177.511 Ashburner J, Friston KJ (2005) Unified segmentation. *Neuroimage* 26:839-851.

512 Bacon SJ, Smith AD (1993) A monosynaptic pathway from an identified vasomotor centre in the

513 medial prefrontal cortex to an autonomic area in the thoracic spinal cord. *Neuroscience*

514 54:719-728.

515 Bandler R, Carrive P (1988) Integrated defence reaction elicited by excitatory amino acid

516 microinjection in the midbrain periaqueductal grey region of the unrestrained cat. *Brain*

517 Res 439:95-106.

518 Bandler R, Shipley MT (1994) Columnar organization in the midbrain periaqueductal gray:

519 modules for emotional expression? *Trends Neurosci* 17:379-389.

520 Barbas H, De Olmos J (1990) Projections from the amygdala to basoventral and mediodorsal

521 prefrontal regions in the rhesus monkey. *J Comp Neurol* 300:549-571.

522 Barbas H, Saha S, Rempel-Clower N, Ghashghaei T (2003a) Serial pathways from primate

523 prefrontal cortex to autonomic areas may influence emotional expression. *BMC*524 *Neuroscienc* 10:25.

- 525 Barbas H, Saha S, Rempel-Clower N, Ghashghaei T (2003b) Serial pathways from primate
526 prefrontal cortex to autonomic areas may influence emotional expression. *BMC Neurosci*
527 4:25.
- 528 Barontini M, Lazzari JO, Levin G, Armando I, Basso SJ (1997) Age-related changes in
529 sympathetic activity: biochemical measurements and target organ responses. *Arch*
530 *Gerontol Geriatr* 25:175-186.
- 531 Barsuglia JP, Kaiser NC, Wilkins SS, Joshi A, Barrows RJ, Paholpak P, Panchal HV, Jimenez
532 EE, Mather MJ, Mendez MF (2014) A scale of socioemotional dysfunction in
533 frontotemporal dementia. *Archives of clinical neuropsychology : the official journal of*
534 *the National Academy of Neuropsychologists* 29:793-805.
- 535 Bates E, Wilson SM, Saygin AP, Dick F, Sereno MI, Knight RT, Dronkers NF (2003) Voxel-
536 based lesion-symptom mapping. *Nat Neurosci* 6:448-450.
- 537 Beissner F, Meissner K, Bar KJ, Napadow V (2013) The autonomic brain: an activation
538 likelihood estimation meta-analysis for central processing of autonomic function. *J*
539 *Neurosci* 33:10503-10511.
- 540 Benarroch EE (1993) The central autonomic network: functional organization, dysfunction, and
541 perspective. *Mayo Clin Proc* 68:988-1001.
- 542 Berntson GG, Bigger JT, Jr., Eckberg DL, Grossman P, Kaufmann PG, Malik M, Nagaraja HN,
543 Porges SW, Saul JP, Stone PH, van der Molen MW (1997) Heart rate variability: origins,
544 methods, and interpretive caveats. *Psychophysiology* 34:623-648.
- 545 Carlson MD, Geha AS, Hsu J, Martin PJ, Levy MN, Jacobs G, Waldo AL (1992) Selective
546 stimulation of parasympathetic nerve fibers to the human sinoatrial node. *Circulation*
547 85:1311-1317.

- 548 Carmichael ST, Price JL (1995) Limbic connections of the orbital and medial prefrontal cortex in
549 macaque monkeys. *Journal of Comparative Neurology* 363:615-641.
- 550 Carmichael ST, Price JL (1996) Connectional networks within the orbital and medial prefrontal
551 cortex of macaque monkeys. *J Comp Neurol* 371:179-207.
- 552 Cohen J (1992) A power primer. *Psychol Bull* 112:155-159.
- 553 Craig AD (2002) How do you feel? Interoception: The sense of the physiological condition of
554 the body. *Nat Rev Neurosci* 3:655-666.
- 555 Craig AD (2005) Forebrain emotional asymmetry: A neuroanatomical basis? *Trends in Cognitive*
556 *Science* 9:566-571.
- 557 Craig AD (2009) How do you feel--now? The anterior insula and human awareness. *Nat Rev*
558 *Neurosci* 10:59-70.
- 559 Critchley HD (2002) Electrodermal responses: what happens in the brain. *Neuroscientist* 8:132-
560 142.
- 561 Critchley HD (2004) The human cortex responds to an interoceptive challenge. *Proceedings of*
562 *the National Academy of Sciences of the United States of America* 101:6333-6334.
- 563 Critchley HD (2005) Neural mechanisms of autonomic, affective, and cognitive integration. *The*
564 *Journal of Comparative Neurology* 493:154-166.
- 565 Critchley HD, Harrison NA (2013) Visceral influences on brain and behavior. *Neuron* 77:624-
566 638.
- 567 Critchley HD, Mathias CJ, Josephs O, O'Doherty J, Zanini S, Dewar BK, Cipolotti L, Shallice T,
568 Dolan RJ (2003) Human cingulate cortex and autonomic control: Converging
569 neuroimaging and clinical evidence. *Brain* 126:2139-2152.

- 570 da Silva LG, de Menezes RC, dos Santos RA, Campagnole-Santos MJ, Fontes MA (2003) Role
571 of periaqueductal gray on the cardiovascular response evoked by disinhibition of the
572 dorsomedial hypothalamus. *Brain Res* 984:206-214.
- 573 Damasio A, Carvalho GB (2013) The nature of feelings: evolutionary and neurobiological
574 origins. *Nat Rev Neurosci* 14:143-152.
- 575 Davis M, Whalen PJ (2001) The amygdala: Vigilance and emotion. *Molecular Psychiatry* 6:13-
576 34.
- 577 Eckart JA, Sturm VE, Miller BL, Levenson RW (2012) Diminished disgust reactivity in
578 behavioral variant frontotemporal dementia. *Neuropsychologia* 50:786-790.
- 579 Enriquez-Geppert S, Eichele T, Specht K, Kugel H, Pantev C, Huster RJ (2013) Functional
580 parcellation of the inferior frontal and midcingulate cortices in a flanker-stop-change
581 paradigm. *Hum Brain Mapp* 34:1501-1514.
- 582 Gatti PJ, Johnson TA, Massari VJ (1996) Can neurons in the nucleus ambiguus selectively
583 regulate cardiac rate and atrio-ventricular conduction? *J Auton Nerv Syst* 57:123-127.
- 584 Ghashghaei HT, Barbas H (2002) Pathways for emotion: interactions of prefrontal and anterior
585 temporal pathways in the amygdala of the rhesus monkey. *Neuroscience* 115:1261-1279.
- 586 Gianaros PJ, Van Der Veen FM, Jennings JR (2004) Regional cerebral blood flow correlates
587 with heart period and high-frequency heart period variability during working-memory
588 tasks: Implications for the cortical and subcortical regulation of cardiac autonomic
589 activity. *Psychophysiology* 41:521-530.
- 590 Giuliani NR, Drabant EM, Bhatnagar R, Gross JJ (2011) Emotion regulation and brain plasticity:
591 expressive suppression use predicts anterior insula volume. *Neuroimage* 58:10-15.

- 592 Goodkind MS, Sturm VE, Ascher EA, Shdo SM, Miller BL, Rankin KP, Levenson RW (2015)
593 Emotion recognition in frontotemporal dementia and Alzheimer's disease: A new film-
594 based assessment. *Emotion* 15:416-427.
- 595 Grossman P, Taylor EW (2007) Toward understanding respiratory sinus arrhythmia: relations to
596 cardiac vagal tone, evolution and biobehavioral functions. *Biol Psychol* 74:263-285.
- 597 Grossman P, van Beek J, Wientjes C (1990) A comparison of three quantification methods for
598 estimation of respiratory sinus arrhythmia. *Psychophysiology* 27:702-714.
- 599 Guo CC, Kurth F, Zhou J, Mayer EA, Eickhoff SB, Kramer JH, Seeley WW (2012) One-year
600 test-retest reliability of intrinsic connectivity network fMRI in older adults. *Neuroimage*
601 61:1471-1483.
- 602 Guo CC, Sturm VE, Zhou J, Gennatas ED, Trujillo AJ, Hua AY, Crawford R, Stables L, Kramer
603 JH, Rankin K, Levenson RW, Rosen HJ, Miller BL, Seeley WW (2016) Dominant
604 hemisphere lateralization of cortical parasympathetic control as revealed by
605 frontotemporal dementia. *Proc Natl Acad Sci U S A* 113:E2430-2439.
- 606 Hoffstaedter F, Grefkes C, Caspers S, Roski C, Palomero-Gallagher N, Laird AR, Fox PT,
607 Eickhoff SB (2014) The role of anterior midcingulate cortex in cognitive motor control:
608 evidence from functional connectivity analyses. *Hum Brain Mapp* 35:2741-2753.
- 609 Hurley KM, Herbert H, Moga MM, Saper CB (1991) Efferent projections of the infralimbic
610 cortex of the rat. *J Comp Neurol* 308:249-276.
- 611 Jennings JR, Sheu LK, Kuan DC, Manuck SB, Gianaros PJ (2016) Resting state connectivity of
612 the medial prefrontal cortex covaries with individual differences in high-frequency heart
613 rate variability. *Psychophysiology* 53:444-454.

- 614 Joshi A, Mendez MF, Kaiser N, Jimenez E, Mather M, Shapira JS (2014a) Skin conductance
615 levels may reflect emotional blunting in behavioral variant frontotemporal dementia. *J*
616 *Neuropsychiatry Clin Neurosci* 26:227-232.
- 617 Joshi A, Barsuglia JP, Mather MJ, Jimenez EE, Shapira J, Mendez MF (2014b) Evaluation of
618 emotional blunting in behavioral variant frontotemporal dementia compared to
619 Alzheimer's disease. *Dement Geriatr Cogn Disord* 38:79-88.
- 620 Kumfor F, Piguet O (2012) Disturbance of emotion processing in frontotemporal dementia: a
621 synthesis of cognitive and neuroimaging findings. *Neuropsychol Rev* 22:280-297.
- 622 Kurth F, Zilles K, Fox PT, Laird AR, Eickhoff SB (2010) A link between the systems: functional
623 differentiation and integration within the human insula revealed by meta-analysis. *Brain*
624 *Structure and Function* 214:519-534.
- 625 Laine CM, Spitzer KM, Mosher CP, Gothard KM (2009) Behavioral triggers of skin conductance
626 responses and their neural correlates in the primate amygdala. *J Neurophysiol* 101:1749-
627 1754.
- 628 Levenson RW, Sturm VE, Haase CM (2014) Emotional and behavioral symptoms in
629 neurodegenerative disease: a model for studying the neural bases of psychopathology.
630 *Annual review of clinical psychology* 10:581-606.
- 631 Levenson RW, Ascher E, Goodkind M, McCarthy M, Sturm V, Werner K (2008) Chapter 25
632 Laboratory testing of emotion and frontal cortex. *Handbook of clinical neurology* 88:489-
633 498.
- 634 Levy MN (1990) Autonomic interactions in cardiac control. *Ann N Y Acad Sci* 601:209-221.

- 635 Levy MN, Yang T, Wallick DW (1993) Assessment of beat-by-beat control of heart rate by the
636 autonomic nervous system: molecular biology techniques are necessary, but not sufficient.
637 *J Cardiovasc Electrophysiol* 4:183-193.
- 638 Masi CM, Hawkley LC, Rickett EM, Cacioppo JT (2007) Respiratory sinus arrhythmia and
639 diseases of aging: obesity, diabetes mellitus, and hypertension. *Biol Psychol* 74:212-223.
- 640 Mendez MF, Fong SS, Shapira JS, Jimenez EE, Kaiser NC, Kremen SA, Tsai PH (2014)
641 Observation of social behavior in frontotemporal dementia. *Am J Alzheimers Dis Other*
642 *Demen* 29:215-221.
- 643 Mesulam MM, Mufson EJ (1982) Insula of the old world monkey. I. Architectonics in the
644 insulo-orbito-temporal component of the paralimbic brain. *Journal of Comparative*
645 *Neurology* 212:1-22.
- 646 Morris JC (1993) The Clinical Dementia Rating (CDR): Current version and scoring rules.
647 *Neurology* 43:2412-2414.
- 648 Mufson EJ, Mesulam MM (1982) Insula of the old world monkey. II: Afferent cortical input and
649 comments on the claustrum. *J Comp Neurol* 212:23-37.
- 650 Nee DE, Wager TD, Jonides J (2007) Interference resolution: insights from a meta-analysis of
651 neuroimaging tasks. *Cogn Affect Behav Neurosci* 7:1-17.
- 652 Nichols TE, Holmes AP (2002) Nonparametric permutation tests for functional neuroimaging: a
653 primer with examples. *Human Brain Mapping* 15:1-25.
- 654 Ongur D, Price JL (2000) The organization of networks within the orbital and medial prefrontal
655 cortex of rats, monkeys, and humans. *Cereb Cortex* 10:206-219.
- 656 Ongur D, An X, Price JL (1998) Prefrontal cortical projections to the hypothalamus in macaque
657 monkeys. *Journal of Comparative Neurology* 401:480-505.

- 658 Oppenheimer SM, Kedem G, Martin WM (1996) Left-insular cortex lesions perturb cardiac
659 autonomic tone in humans. *Clinical Autonomic Research* 6:131-140.
- 660 Oppenheimer SM, Gelb A, Girvin JP, Hachinski VC (1992) Cardiovascular effects of human
661 insular cortex stimulation. *Neurology* 42:1727-1732.
- 662 Porges SW (2001) The polyvagal theory: phylogenetic substrates of a social nervous system.
663 *International journal of psychophysiology : official journal of the International*
664 *Organization of Psychophysiology* 42:123-146.
- 665 Price JL (1999) Prefrontal cortical networks related to visceral function and mood. *Ann N Y*
666 *Acad Sci* 877:383-396.
- 667 Rascovsky K, Hodges JR, Kipps CM, Johnson JK, Seeley WW, Mendez MF, Knopman D,
668 Kertesz A, Mesulam M, Salmon DP, Galasko D, Chow TW, Decarli C, Hillis A, Josephs
669 K, Kramer JH, Weintraub S, Grossman M, Gorno-Tempini ML, Miller BL (2007)
670 Diagnostic criteria for the behavioral variant of frontotemporal dementia (bvFTD):
671 Current limitations and future directions. *Alzheimer Disease and Associated Disorders*
672 21:S14-S18.
- 673 Rybak IA, Shevtsova NA, Paton JF, Dick TE, St-John WM, Morschel M, Dutschmann M (2004)
674 Modeling the ponto-medullary respiratory network. *Respiratory physiology &*
675 *neurobiology* 143:307-319.
- 676 Saku K, Kishi T, Sakamoto K, Hosokawa K, Sakamoto T, Murayama Y, Kakino T, Ikeda M, Ide
677 T, Sunagawa K (2014) Afferent vagal nerve stimulation resets baroreflex neural arc and
678 inhibits sympathetic nerve activity. *Physiological reports* 2.
- 679 Saper CB (2002) The central autonomic nervous system: Conscious visceral perception and
680 autonomic pattern generation. *Annual Review of Neuroscience* 25:433-469.

- 681 Saper CB, Loewy AD, Swanson LW, Cowan WM (1976) Direct hypothalamo-autonomic
682 connections. *Brain Res* 117:305-312.
- 683 Satterthwaite TD, Elliott MA, Gerraty RT, Ruparel K, Loughead J, Calkins ME, Eickhoff SB,
684 Hakonarson H, Gur RC, Gur RE, Wolf DH (2013) An improved framework for confound
685 regression and filtering for control of motion artifact in the preprocessing of resting-state
686 functional connectivity data. *Neuroimage* 64:240-256.
- 687 Seeley WW, Zhou J, Kim EJ (2012) Frontotemporal dementia: What can the behavioral variant
688 teach us about human brain organization? *Neuroscientist* 18:373-385.
- 689 Seeley WW, Crawford R, Rascovsky K, Kramer JH, Weiner M, Miller BL, Gorno-Tempini ML
690 (2008) Frontal paralimbic network atrophy in very mild behavioral variant
691 frontotemporal dementia. *Arch Neurol* 65:249-255.
- 692 Seeley WW, Menon V, Schatzberg AF, Keller J, Glover GH, Kenna H, Reiss AL, Greicius MD
693 (2007) Dissociable intrinsic connectivity networks for salience processing and executive
694 control. *Journal of Neuroscience* 27:2349-2356.
- 695 Shipley MT (1982) Insular cortex projection to the nucleus of the solitary tract and brainstem
696 visceromotor regions in the mouse. *Brain Res Bull* 8:139-148.
- 697 Shirer WR, Ryali S, Rykhlevskaia E, Menon V, Greicius MD (2012) Decoding subject-driven
698 cognitive states with whole-brain connectivity patterns. *Cereb Cortex* 22:158-165.
- 699 Sturm VE, Ascher EA, Miller BL, Levenson RW (2008) Diminished self-conscious emotional
700 responding in frontotemporal lobar degeneration patients. *Emotion* 8:861-869.
- 701 Sturm VE, Allison SC, Rosen HJ, Miller BL, Levenson RW (2006) Self-conscious emotion
702 deficits in frontotemporal lobar degeneration. *Brain* 129:2508-2516.

- 703 Sturm VE, Sollberger M, Seeley WW, Rankin KP, Ascher EA, Rosen HJ, Miller BL, Levenson
704 RW (2013) Role of right pregenual anterior cingulate cortex in self-conscious emotional
705 reactivity. *Soc Cogn Affect Neurosci* 8:468-474.
- 706 ter Horst GJ, Luiten PG, Kuipers F (1984) Descending pathways from hypothalamus to dorsal
707 motor vagus and ambiguus nuclei in the rat. *J Auton Nerv Syst* 11:59-75.
- 708 Thayer JF, Lane RD (2000) A model of neurovisceral integration in emotion regulation and
709 dysregulation. *J Affect Disord* 61:201-216.
- 710 Thayer JF, Siegle GJ (2002) Neurovisceral integration in cardiac and emotional regulation. *IEEE*
711 *Eng Med Biol Mag* 21:24-29.
- 712 Thayer JF, Ahs F, Fredrikson M, Sollers JJ, 3rd, Wager TD (2012) A meta-analysis of heart rate
713 variability and neuroimaging studies: implications for heart rate variability as a marker of
714 stress and health. *Neurosci Biobehav Rev* 36:747-756.
- 715 Touroutoglou A, Hollenbeck M, Dickerson BC, Feldman Barrett L (2012) Dissociable large-
716 scale networks anchored in the right anterior insula subserve affective experience and
717 attention. *Neuroimage* 60:1947-1958.
- 718 Varikuti DP, Hoffstaedter F, Genon S, Schwender H, Reid AT, Eickhoff SB (2017) Resting-state
719 test-retest reliability of a priori defined canonical networks over different preprocessing
720 steps. *Brain Struct Funct* 222:1447-1468.
- 721 Winkelmann T, Thayer JF, Pohlack S, Nees F, Grimm O, Flor H (2016) Structural brain
722 correlates of heart rate variability in a healthy young adult population. *Brain Struct Funct*.
- 723 Wittling W, Block A, Genzel S, Schweiger E (1998a) Hemisphere asymmetry in
724 parasympathetic control of the heart. *Neuropsychologia* 36:461-468.

AUTONOMIC NETWORK ARCHITECTURE

- 725 Wittling W, Block A, Schweiger E, Genzel S (1998b) Hemisphere asymmetry in sympathetic
726 control of the human myocardium. *Brain Cogn* 38:17-35.
- 727 Xavier CH, Beig MI, Ianzer D, Fontes MA, Nalivaiko E (2013) Asymmetry in the control of
728 cardiac performance by dorsomedial hypothalamus. *American journal of physiology*
729 *Regulatory, integrative and comparative physiology* 304:R664-674.
- 730 Yoon BW, Morillo CA, Cechetto DF, Hachinski V (1997) Cerebral hemispheric lateralization in
731 cardiac autonomic control. *Arch Neurol* 54:741-744.
- 732 Zhou J, Greicius MD, Gennatas ED, Growdon ME, Jang JY, Rabinovici GD, Kramer JH, Weiner
733 M, Miller BL, Seeley WW (2010) Divergent network connectivity changes in
734 behavioural variant frontotemporal dementia and Alzheimer's disease. *Brain* 133:1352-
735 1367.
- 736

737

Acknowledgments

738 The authors would like to thank the patients, healthy controls, and their families for participating
739 in our research studies. This project was supported by grants from the NIH National Institute on
740 Aging (P50AG023501, P01AG019724, R01AG052496, R01AG032306, R01AG057204,
741 1K23AG040127, and 1K23AG045289), The Larry L. Hillblom Foundation (2013-A-029-SUP
742 and 2005/2T), the John Douglas French Foundation, the Consortium for Frontotemporal
743 Dementia Research, and the Tau Consortium.

744

745

746 Table 1

747 *Participant characteristics classified by diagnostic group.* Means (*M*) and standard deviations
 748 (*SD*) are listed for each group unless otherwise noted. Neuropsychological testing included
 749 assessment of verbal and visual episodic memory, executive function (e.g., set-shifting, working
 750 memory, and fluency), language, and visuospatial functioning. A total of 19/23 patients and
 751 17/24 HC completed neuropsychological testing in close proximity (within 4 months for patients
 752 and 12 months for the HC) to the laboratory assessment. The CDR Total and Sum of the Boxes
 753 were computed for each participant with higher scores indicating greater impairment. bvFTD=
 754 behavioral variant frontotemporal dementia, BMI= Body Mass Index, CDR Total= Clinical
 755 Dementia Rating Total score, CDR-SB= Clinical Dementia Rating Sum of Boxes, HC= healthy
 756 controls, and MMSE= Mini-Mental State Examination. † The HC received the California Verbal
 757 Learning Test-II (16-word list) instead of the Short Form. Their performance on the 20-minute
 758 delay was also in the average range ($M= 13.6$, $SD= 2.1$). We used analysis of variance and chi-
 759 square tests, when appropriate, to examine group differences. Partial eta squared (η_p^2) is
 760 provided as a measure of effect size.

	<i>bvFTD</i> <i>M(SD)</i>	<i>HC</i> <i>M(SD)</i>	<i>p</i>	η_p^2
N	23	24		
Age	58.4 (8.4)	67.9 (5.4)	<.001	.31
Sex: % Female	30.4	54.2	.10	
Education	15.7 (2.9)	17.6 (2.3)	.02	.12
Handedness: % Right-handed	100.0	91.7	.16	
BMI	32.2 (29.1)	25.8 (12.3)	.37	.02
CDR Total	1.2 (0.6)	0.0 (0.0)	<.001	.72

AUTONOMIC NETWORK ARCHITECTURE

CDR-SB	7.2 (2.8)	0.0 (0.0)	<.001	.77
MMSE	23.9 (5.2)	29.6 (0.6)	<.001	.38
California Verbal Learning Test- Short Form 10-Minute Recall (/9)	3.8 (2.3)	†		
Benson Figure Copy 10-Minute Recall (/17)	6.8 (4.4)	11.4 (2.6)	.001	.29
Modified Trails (correct lines per minute)	13.9 (13.0)	39.6 (12.1)	<.001	.53
Modified Trails Errors	2.4 (2.4)	0.2 (0.4)	.001	.31
Phonemic Fluency (# correct in 60 seconds)	5.5 (3.8)	19.2 (4.3)	<.001	.76
Semantic Fluency (# correct in 60 seconds)	9.1 (4.7)	24.0 (5.3)	<.001	.70
Design Fluency Correct (# correct in 60 seconds)	4.8 (3.3)	11.8 (2.8)	<.001	.58
Design Fluency Repetitions	7.3 (6.3)	1.8 (2.4)	.001	.26
Digits Backward	3.2 (0.9)	6.0 (1.4)	<.001	.61
Benson Figure Copy (/17)	13.8 (2.1)	15.3 (1.0)	.015	.16
Calculations (/5)	3.3 (1.1)	4.9 (0.2)	<.001	.54
Boston Naming Test Spontaneous Correct (/15)	11.8 (3.1)	14.6 (0.7)	<.001	.30
Peabody Picture Vocabulary Test (/16)	13.7 (3.3)	15.7 (0.6)	.025	.15

761

762 Table 2

763 *Resting baseline physiological levels.* Analyses of covariance (controlling for age, sex, and
 764 education) found that patients with bvFTD (n=22) had significantly lower respiratory sinus
 765 arrhythmia, lower skin conductance level, and shorter respiration period than the healthy controls
 766 (n=22). When we added additional covariates that might influence RSA (i.e., resting inter-beat
 767 interval, resting respiration period, and body mass index) to the model (while also controlling for
 768 education, sex, and age), patients continued to have lower RSA, $F(1, 33)= 469, p= .038, \eta_p^2= .13$.
 769 For SCL, although including resting inter-beat interval, resting respiration period, and body mass
 770 index as additional covariates caused the difference to fall to trend levels, the pattern of results
 771 was in the expected direction, with patients having lower SCL than controls, $F(1, 32)= 2.82, p<$
 772 $.11, \eta_p^2= .08$. To examine whether the results of the original model (controlling for age, sex, and
 773 education) held in a smaller, age-matched sample, we removed patients under age 58 (n=6) and
 774 healthy controls over age 70 (n=8). In this subset of participants (17 bvFTD and 15 HC), the
 775 patients and controls did not differ in age, $F(1,31)=3.2, p=.09, \eta_p^2=.09$. In this smaller sample, the
 776 group differences in baseline autonomic activity remained significant. Compared to healthy
 777 controls, patients with bvFTD had lower RSA, $F(1,27)=5.6, p=.03, \eta_p^2=.17$, lower SCL,
 778 $F(1,27)=4.2, p= .05, \eta_p^2=.14$, and shorter respiration period, $F(1,27)=8.1, p= .008, \eta_p^2=.23$. Means
 779 (M) and standard deviations (SD) are reported. Partial eta squared (η_p^2) is provided as a measure
 780 of effect size. * indicates significant differences at $p< .05$ in the first model described above.

<i>bvFTD</i>	<i>Healthy</i>			
<i>M(SD)</i>	<i>Controls</i>	<i>F</i>	<i>p</i>	η_p^2
	<i>M(SD)</i>			

AUTONOMIC NETWORK ARCHITECTURE

Inter-beat interval (ms)	906.6 (156.74)	981.9 (133.9)	0.3	.57	.01
Respiratory sinus arrhythmia (ms)*	39.1 (22.9)	62.9 (55.3)	10.0	.003	.20
Skin conductance level (μ mhos)*	2.0 (0.9)	2.9 (1.7)	4.6	.037	.10
Respiration period (ms)*	4035.6 (915.5)	4750.3 (946.6)	9.4	.004	.19
Finger temperature ($^{\circ}$ F)	80.7 (5.5)	80.5 (5.6)	0.0	.97	.00

781

782

783 Table 3

784 *Anatomical correlates of baseline PANS and SANS activity.* Whole-brain VBM analyses in
 785 patients with bvFTD (controlling for age, sex, and education) revealed that atrophy in many ANS
 786 network nodes was associated with lower baseline RSA (n=21) and SCL (n=20). Montreal
 787 Neurological Institute coordinates (x, y, z) given for maximum *T*-score for the cluster (cluster
 788 size > 150 mm³). Results are significant at $p < .001$, uncorrected. † denotes significance at $p_{\text{FWE}} <$
 789 .05. To identify the independent neural correlates of PANS and SANS activity, we conducted
 790 follow-up VBM analyses when controlling for the opposing autonomic measure (i.e., including
 791 SCL as an additional covariate in the RSA VBM analysis and SCL as an additional covariate in
 792 the RSA VBM analysis). * denotes significance at $p < .001$, uncorrected, when also controlling
 793 for the opposing autonomic measure.

<i>Anatomical Region</i>	<i>Cluster Volume (mm³)</i>	<i>x</i>	<i>y</i>	<i>z</i>	<i>Maximum T-score</i>	<i>β</i>
RSA						
Left ventral anterior insula*	1312	-41	12	-15	5.41	.79
Left inferior temporal lobe*	448	-32	2	-36	4.96	.59
Right parahippocampal gyrus	320	15	11	-30	4.50	.63
Left parahippocampal gyrus*	168	-14	8	-26	4.28	.68
SCL						
Left inferior temporal gyrus†*	6120	-51	-21	-27	6.57	.77
Left temporal pole*	1528	-33	9	-50	5.02	.72
Right fusiform gyrus*	1200	27	-15	-41	5.05	.69
Left precentral gyrus	1160	-41	-18	59	4.31	.75
Left dorsal mid-insula*	1088	-36	14	15	7.08	.61
Left orbitofrontal cortex*	1080	-21	18	-16	4.71	.65
Left orbitofrontal cortex*	1080	-18	47	-21	5.34	.67
Right orbitofrontal cortex*	912	26	21	-11	5.16	.54
Right frontal pole*	880	8	71	14	5.77	.81
Right frontal pole	776	-15	69	-11	5.38	.67
Left parahippocampal gyrus*	712	-11	-8	-35	5.60	.79

AUTONOMIC NETWORK ARCHITECTURE

Right middle frontal gyrus*	672	50	14	51	6.20	.89
Left superior frontal gyrus	600	-17	41	51	4.65	.81
Right postcentral gyrus	584	23	-30	74	4.25	.76
Right precentral gyrus*	496	44	-20	60	4.30	.69
Left precuneus	424	-17	-41	71	4.94	.70
Left frontal pole*	424	-38	56	9	4.30	.66
Left hypothalamus	424	-8	-5	-9	4.14	.60
Left fusiform gyrus	416	-33	-17	-44	4.17	.73
Right gyrus rectus	352	9	33	-17	4.16	.54
Right precentral gyrus	320	35	-8	62	4.75	.80
Left fusiform gyrus	304	51	-11	-29	4.33	.60
Left inferior parietal lobe	280	-47	-50	54	4.29	.73
Right superior frontal gyrus*	280	23	57	36	5.16	.67
Left precentral gyrus*	264	-32	-9	63	4.33	.77
Right cerebellum*	232	35	-50	-45	4.02	.50
Left pars triangularis	200	-33	33	3	4.09	.75
Right inferior parietal lobe	192	48	-42	59	4.38	.66
Left supplementary motor area	160	-9	8	65	4.61	.63

794

795

796

797

798 Table 4

799 *Node-pair connections (i.e. edges) that explained a significant portion of variance in RSA and*
 800 *SCL in the regression analyses.* Forward-entry hierarchical regression analyses in 15 patients
 801 with bvFTD and 13 healthy controls (controlling for age, sex, education, and diagnosis) were
 802 used to determine which edges were significant predictors of baseline PANS and SANS. Edges
 803 with positive and negative associations with RSA and SCL entered the models, suggesting that a
 804 combination of strong and weak functional connectivity in the ANS network is necessary for
 805 resting physiological activity. † denotes edge that lost significance when controlling for mean
 806 resting respiration period and inter-beat interval. * denotes edges that lost significance when
 807 controlling for the mean gray matter volume of the nodes in that edge.

<i>Edge Category</i>	<i>Edge Label</i>	<i>Zero-order Correlation</i>	β	R^2 Change	<i>p-value of F Change</i>
RSA					
<i>Positive Correlation</i>					
Left vAI –	2–5	.41	.48	.22	.002
Left ACC					
Left vAI –	2–16	.33	.51	.14	.01
Right ACC †					
Right vAI –	13–15	.29	.83	.12	.03
Right ACC					

AUTONOMIC NETWORK ARCHITECTURE

<i>Negative Correlation</i>						
Left ACC –	7–9	-.57	-.56	.20	.01	
Left Hypothalamus						
Left ACC –	7–19	-.57	-.52	.30	.001	
Right Hypothalamus						
Right ACC –	16–19	-.33	-.37	.12	.01	
Right Hypothalamus†						
Right vAI1 –	12–13	-.32	-.61	.09	.04	
Right vAI2						
Right ACC –	17–19	-.30	-.43	.06	.04	
Right Hypothalamus*						
Right vAI –	13–19	-.26	.11	.21	.01	
Right Hypothalamus†*						
Right vAI –	12–17	-.25	-.32	.06	.01	
Right ACC†						
Left ACC –	6–18	-.22	-.42	.09	.02	
Right Amygdala†						
SCL						
<i>Positive Correlation</i>						
Left ACC –	6–19	.31	.65	.14	.02	
Right Hypothalamus						
Right ACC –	16–18	.23	.38	.08	.04	
Right Amygdala						
<i>Negative Correlation</i>						
Left dAI –	1–21	-.37	-.54	.25	.003	

AUTONOMIC NETWORK ARCHITECTURE

PAG					
Right vAI1 –	12–13	-.31	-.39	.10	.03
Right vAI2					
Right ACC –	17–5	-.30	-.40	.12	.01
Left ACC					
Right dAI –	11–21	-.28	-.71	.25	.003
PAG					
Left aMCC –	4–19	-.20	-.59	.16	.02
Right Hypothalamus					

808

809

810 Table 5

811 *Edge weight connectivity strength in bvFTD versus healthy controls.* Mean connectivity
 812 strengths of the edges that entered the RSA and SCL regression models for bvFTD (n=15) and
 813 healthy control (n=14) groups.

<i>Edge Category</i>	<i>Edge Label</i>	<i>bvFTD M (SD)</i>	<i>Healthy Controls M (SD)</i>	<i>T</i>	<i>p</i>
RSA					
<i>Positive Correlation</i>					
Left vAI –	2–5	.40	.46	-1.17	.25
Left ACC		(.28)	(.31)		
Left vAI –	2–16	.41	.49	-0.77	.45
Right ACC		(.29)	(.24)		
Right vAI –	13–15	.44	.51	-2.42	.02
Right ACC		(.29)	(.28)		
<i>Negative Correlation</i>					
Left ACC –	7–9	.17	.14	-0.01	.99
Left Hypothalamus		(.31)	.25)		
Left ACC –	7–19	.14	.20	0.08	.94
Right Hypothalamus		(.25)	(.17)		
Right ACC –	16–19	.13	.32	1.43	.17
Right Hypothalamus		(.24)	(.19)		

AUTONOMIC NETWORK ARCHITECTURE

Right vAI1 –	12–13	.66	.66	-0.17	.87
Right vAI2		(.26)	(.25)		
Right ACC –	17–19	.12	.28	0.22	.83
Right Hypothalamus		(.26)	(.18)		
Right vAI –	13–19	.20	.35	0.30	.77
Right Hypothalamus		(.24)	(.21)		
Right vAI –	12–17	.31	.33	-0.73	.47
Right ACC		(.28)	(.22)		
Left ACC –	6–18	.20	.41	-2.28	.03
Right Amygdala		(.24)	(.34)		
SCL					
<i>Positive Correlation</i>					
Left ACC –	6–19	.11	.37	-2.04	.05
Right Hypothalamus		(.23)	(.17)		
Right ACC –	16–18	.18	.39	-2.14	.04
Right Amygdala		(.18)	(.33)		
<i>Negative Correlation</i>					
Left dAI –	1–21	.06	.12	-1.04	.31
PAG		(.27)	(.32)		
Right vAI1 –	12–13	.66	.66	-0.17	.86
Right vAI2		(.26)	(.25)		
Right ACC –	17–5	.47	.52	-2.21	.04
Left ACC		(.19)	(.25)		
Right dAI –	11–21	-.05	.15	-2.31	.03
PAG		(.22)	(.24)		

AUTONOMIC NETWORK ARCHITECTURE

Left aMCC –	4–19	.14	.36	-2.24	.04
Right Hypothalamus		(.25)	(.22)		

814

815 Legends

816 Figure 1

817 *Anatomical framework of autonomic functioning and relevant ROIs.* (A) Building on previous
818 studies, we developed a lateralized schematic of parasympathetic autonomic nervous system
819 (PANS) and sympathetic autonomic nervous system (SANS) functioning. The salience network
820 is anchored by hubs in anterior insula (AI) and anterior cingulate cortex (ACC) and has tight
821 connections with central pattern generators including the amygdala, hypothalamus, and
822 periaqueductal gray. Although this framework does not include many brainstem regions that are
823 also integral for ANS activity (e.g., nucleus of the solitary tract, parabrachial nucleus, nucleus
824 ambiguus, dorsal motor nucleus of the vagus, and rostral ventrolateral medulla, among others), it
825 does include critical cortical and subcortical regions that can be measured with neuroimaging
826 techniques. Thus, this represents a simplified yet testable conceptualization of the neural system
827 that supports resting physiological activity as well as phasic emotional reactions. (B) We
828 extracted the BOLD time series from 21 ROIs that pertained to our neuroanatomical model of
829 ANS functioning. Connectivity strength between each node-pair (or edge) was calculated by
830 correlating the BOLD time series of each ROI with the BOLD time series of every other ROI,
831 which provided us with a matrix of 210 edges to correlate with measures of baseline RSA and
832 SCL. The ROIs were functionally connected to the insula and were obtained from task-free fMRI
833 data in an independent cohort of healthy older controls. These ROIs (with the numerical labels
834 that we assigned to them denoted in parentheses) included: left dorsal AI (1), right dorsal AI
835 (11), left ventral AI node 1 (2), right ventral AI node 1 (12), left ventral AI node 2 (3), right
836 ventral AI node 2 (13), left anterior midcingulate cortex (4), right anterior midcingulate cortex
837 (14), left pregenual ACC node 1 (5), right pregenual ACC node 1 (15), left pregenual ACC node

AUTONOMIC NETWORK ARCHITECTURE

838 2 (6), right pregenual ACC node 2 (16), left subgenual ACC (7), right subgenual ACC (17), left
839 amygdala (8), right amygdala (18), left hypothalamus (9), right hypothalamus (19), left thalamus
840 (10), right thalamus (20), periaqueductal gray (21). AI = anterior insula, ACC = anterior
841 cingulate cortex, aMCC = anterior midcingulate cortex, Amy = amygdala, dAI = dorsal anterior
842 insula, Hyp = hypothalamus, PAG = periaqueductal gray, Thal = thalamus, and vAI = ventral
843 anterior insula.

844 Figure 2

845 *Baseline PANS activity is determined by the strength of certain salience network connections*
846 *and the suppression of others.* (A) Atrophy in left vAI was associated with lower RSA at $p <$
847 $.001$, uncorrected (controlling for age, sex, and education) in 21 patients with bvFTD. Cyan
848 represents T -scores at $p < .001$, uncorrected ($T > 3.69$), and green represents t -scores at $p < .005$,
849 uncorrected ($T > 2.92$). (B) We conducted a follow-up VBM analysis of RSA in which we added
850 SCL as an additional covariate to the model. The results remained largely unchanged though
851 some weaker clusters no longer remained significant. Cyan represents T -scores at $p < .001$,
852 uncorrected ($T > 3.79$), and green represents T -scores at $p < .005$, uncorrected ($T > 2.98$). (C) The
853 fMRI analyses revealed that lower baseline PANS activity was associated with lower vFI – ACC
854 connectivity and higher connectivity primarily in ACC – hypothalamus/amygdala. Line
855 thickness is scaled to reflect the percentage of variance that each edge explained (i.e., R^2 change,
856 which ranged from .06 to .30) in the hierarchical regression model. Statistical maps are
857 superimposed on the Montreal Neurological Institute template brain.

858 Figure 3

859 *Baseline SANS activity is determined by the strength of certain salience network connections and*
860 *the suppression of others.* (A) Atrophy in inferior temporal gyrus, dorsal mid-insula, and
861 hypothalamus was associated with lower SCL at $p < .001$, uncorrected (controlling for age, sex,
862 and education) in 20 patients with bvFTD. At more permissive thresholds ($p < .005$, uncorrected),
863 smaller volume in the amygdala and PAG was also associated with lower SCL. The inferior
864 temporal gyrus was the only cluster that survived permutation analysis, $p_{FWE} < .05$. Cyan
865 represents T -scores at $p < .001$, uncorrected ($T > 3.73$), and green represents t -scores at $p < .005$,
866 uncorrected ($T > 2.95$). (B) We conducted a follow-up VBM analysis of SCL in which we added
867 RSA as an additional covariate to the model. The results remained largely unchanged though
868 some weaker clusters no longer remained significant. Blue represents T -scores at $p < .001$,
869 uncorrected ($T > 3.79$), and green represents T -scores at $p < .005$, uncorrected ($T > 2.98$). (C)
870 Baseline SANS deficits were associated with lower connectivity in right amygdala/hypothalamus
871 edges and higher connectivity primarily in bilateral dAI – PAG edges. Line thickness is scaled to
872 reflect the percentage of variance that each edge explained (i.e., R^2 change, which ranged from
873 .08 to 25) in the hierarchical regression model. Statistical maps are superimposed on the
874 Montreal Neurological Institute template brain.

875 Figure 4

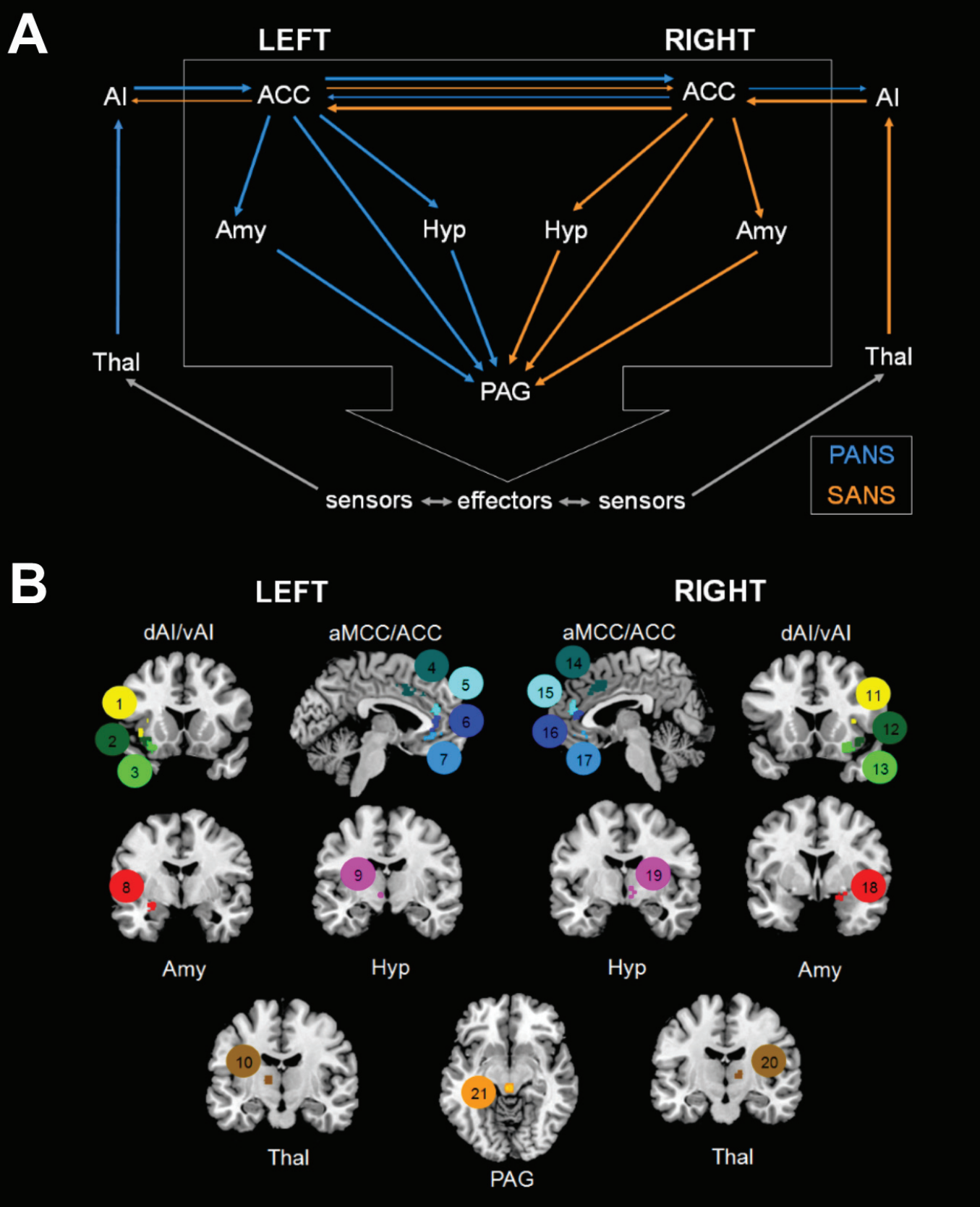
876 *Regression Plots for the Functional Imaging Analyses.* Partial residual plots for the four edges
877 that explained the greatest percentage of variance (R^2 change) in RSA and SCL (controlling for
878 age, sex, education, and diagnosis). Higher resting RSA was associated with (A) greater left vAI
879 – left ACC (edge 2–5) and (B) lower left ACC – right hypothalamus (edge 7–19) functional
880 connectivity. Higher SCL was associated with (C) greater left ACC – right hypothalamus (edge
881 6–19) and (D) lower right dAI – PAG (edge 11–21) functional connectivity. Given that we

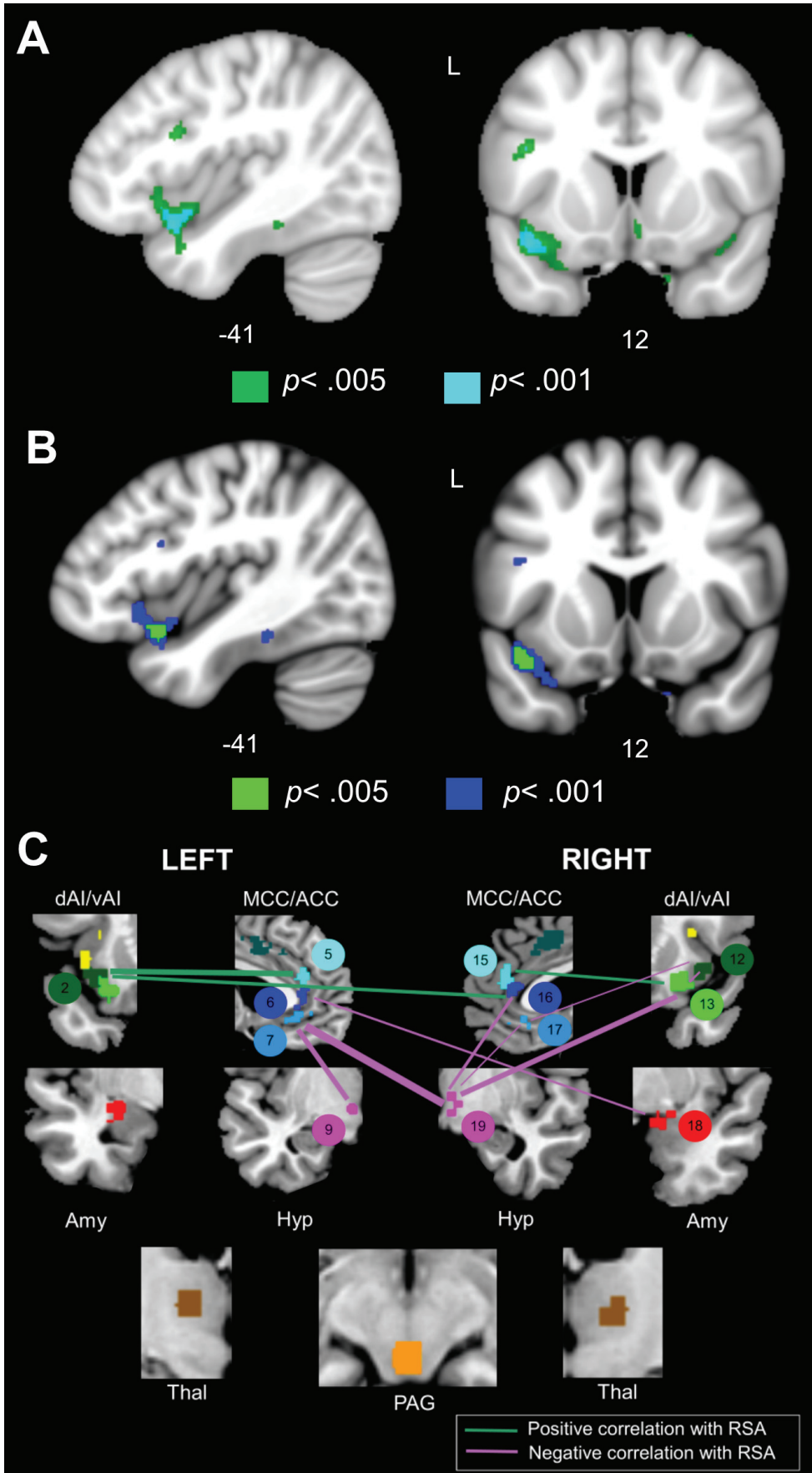
882 controlled for diagnosis in the regression models, these plots show that the association that we
883 detected between edge connectivity and resting autonomic activity were present in both
884 diagnostic groups and thus, were not driven by group membership. When we repeated the
885 original analyses in each diagnosis separately, RSA and SCL had similar associations with the
886 functional connectivity measures (Figure 4-1). See Figure 1 for abbreviations.

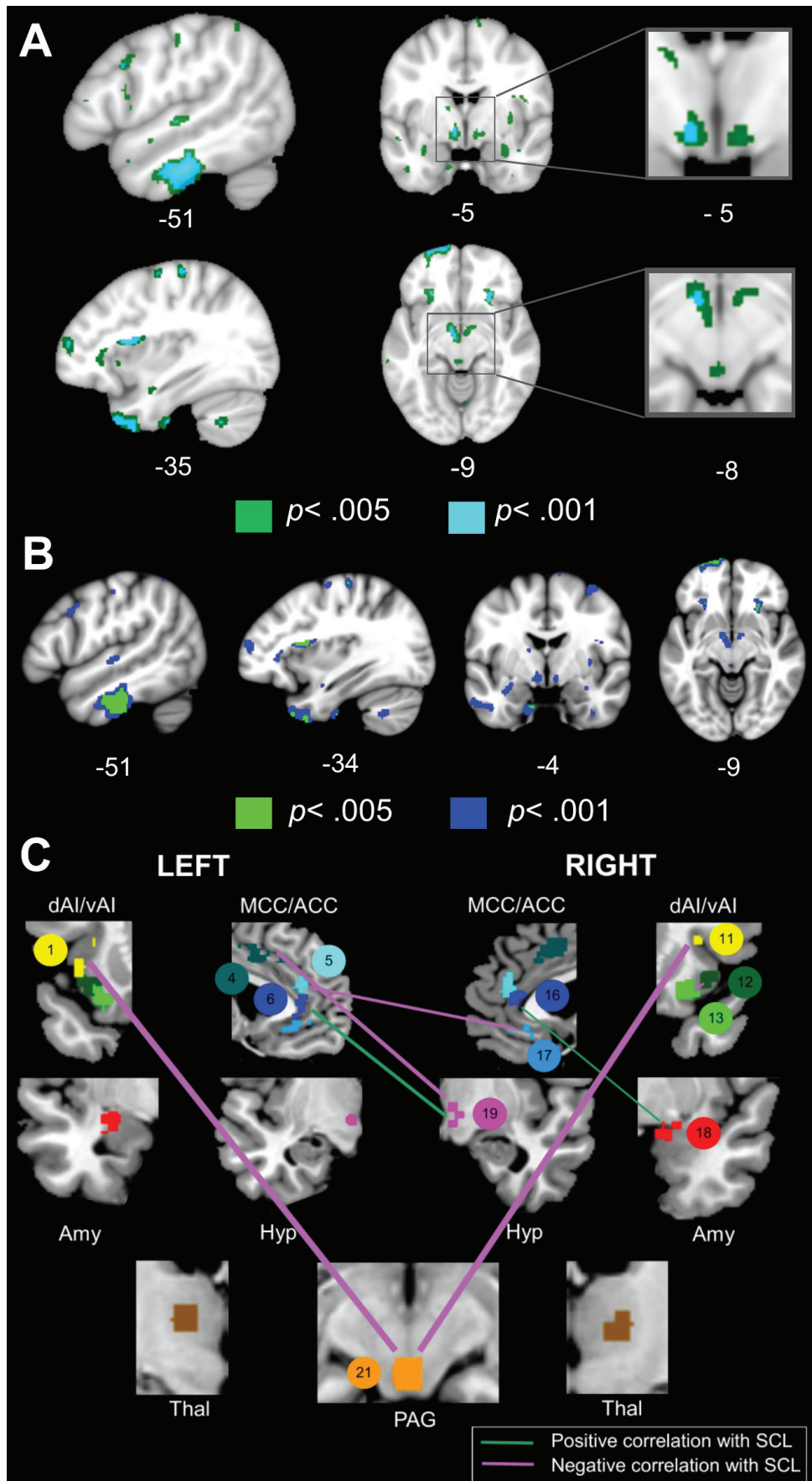
887 Figure 5

888 *Hypothesized RSA network.* Our results suggest that resting PANS tone depends on the integrity
889 of both strong and weak edges in the salience network. Stronger vAI – ACC connectivity and
890 weaker ACC – hypothalamus/amygdala connectivity was associated with higher resting RSA.
891 RSA, therefore, depends on intact connections between vAI (left > right) and ACC and weaker
892 connections between ACC and hypothalamus/amygdala (right > left), suggesting that nodes that
893 support SANS outflow must be inhibited to facilitate PANS activity. We hypothesize that PANS-
894 specific (e.g., ventrolateral PAG) and SANS-specific (e.g., dorsal PAG) subregions in each node
895 as well as untested connections with brainstem nuclei that are difficult to image (e.g., nucleus
896 ambiguus) may also play important roles in this network that we were not able to evaluate. Green
897 lines are edges in which stronger connectivity promoted RSA (i.e., edges 2–5, 2–16, and 13–15),
898 and purple lines are edges in which stronger connectivity inhibited RSA (i.e., 13–19, 7–9, 16–19,
899 17–19, and 6–18). * indicates edges that emerged as significant predictors of RSA in the
900 regression models. Laterality has been omitted for visual simplicity but is alluded to in the figure
901 layout. dPAG = dorsal PAG, vIPAG = ventrolateral PAG. See Figure 1 for other abbreviations.

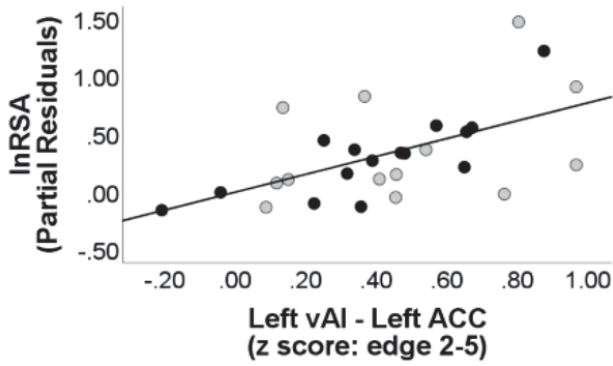
902



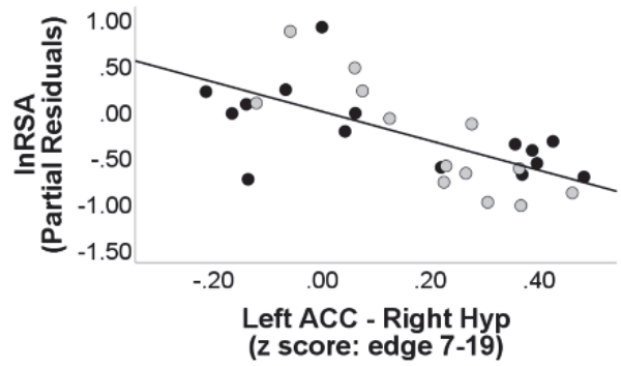




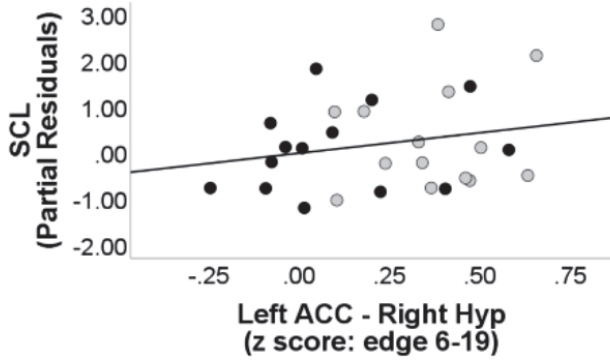
A Positive Correlation with RSA



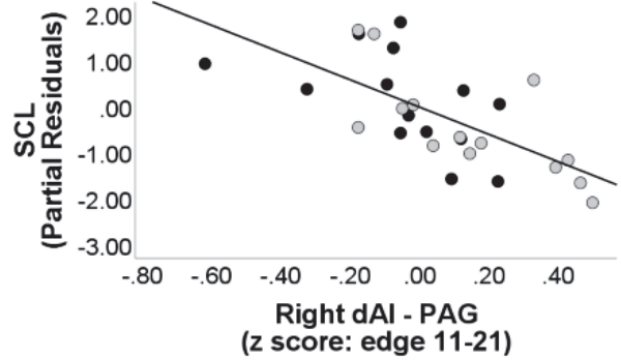
B Negative Correlation with RSA



C Positive Correlation with SCL



D Negative Correlation with SCL



Diagnosis



bvFTD



HC

